JOURNAL OF APPLIED ELECTROCHEMISTRY 17 (1987) 821–827

Hetero-epitaxial growth of zinc electrodeposits on low-carbon steel sheets

KAZUHITO KAMEI, YASUYA OHMORI

Technical Research Laboratories, Sumitomo Metal Industries, Ltd, Nishinagasu-Hondori, Amagasaki 660, Japan

Received 21 October 1986; revised 28 November 1986

Crystallographic aspects of the electrodeposition of zinc on low-carbon steel sheets have been examined with particular emphasis on the hetero-epitaxy. The hetero-epitaxial growth of zinc crystals largely depends on the surface condition of the ferrite substrate and occurs even at a current density as high as 2 A cm^{-2} by reducing the surface oxidation layer. The surface roughness of the substrate induces local disturbance in hetero-epitaxial growth. The orientation relationship between zinc crystals and the ferrite substrate can be interpreted in terms of the minimum misfit atomic arrangements between both phases.

1. Introduction

Crystallographic aspects of the zinc electrodeposits such as the hetero-epitaxy between the deposits and the substrate have been the subjects of numerous investigations since the experiments of Bockris *et al.* [1]. The substrates so far examined are zinc [1, 2], copper [2], aluminium [3, 4] and iron [5]. In all the cases reported, although hetero-epitaxial growth of zinc deposits occurred at lower cathodic overpotential, it disappeared at higher cathodic overpotential.

Hetero-epitaxial growth, which is the continuation of substrate structure by deposits, is favoured when the substrate surface is atomically clean and the direct atomic interaction between deposits and substrate can occur. The surface condition of the substrate such as the adsorption of oxygen atoms or the surface oxidation affects the occurrence of hetero-epitaxy. This is also of practical importance in the production of electrogalvanized steel sheets.

Thus, in the present study the effects of substrate surface condition on the hetero-epitaxy of zinc electrodeposits on low carbon steel sheets were examined.

2. Experimental procedure

The substrates used were annealed, low-carbon steel sheets containing 0.05 wt % carbon and large-grained, high-purity iron sheets prepared by a strain annealing method. These substrates were punched into discs, 15 mm in diameter, and were fixed onto copper sheets, 300 mm wide and 120 mm long, by insulating tapes. The central area of diameter 9 mm was uncovered and acted as cathode during the electrodeposition.

A platinum counter electrode, which was similarly fixed onto a copper sheet, was placed parallel to the cathode. The distance between the anode and the cathode was 20 mm.

Three different surface preparations of the 0.05 wt % steel substrates were employed. In the first case the substrates were electrolysed anodically in 2.5 M NaOH solution for 20 s at a current density of 5 mA cm^{-2}, and were rinsed in distilled water. They were then soaked in 3.4 M HCl solution for 1 min to remove the iron oxide film formed during the electrolysis. They were again rinsed in distilled water and dried in air at room temperature. These substrates are referred to as substrate A. In the second case, however, substrates prepared in the same way as substrate A from the electrolysis to the final rinsing were not dried but were covered with a water film until the subsequent transfer into the plating solution. These are referred to as substrate B. In the third case the substrates were chemically polished at boiling temperature in 5.8 M H_2O_2

0021–891X/87 $03.00 + .12

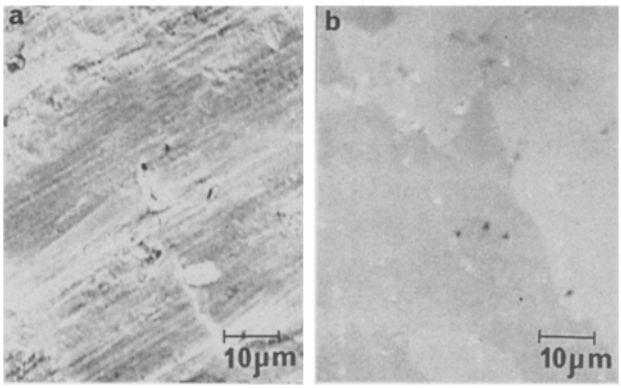

Fig. 1. SEM micrograph of the substrate surfaces. (a) Substrate A; (b) substrate C.

solution saturated with oxalic acid, and are referred to as substrate C. This chemical polishing provides very smooth surfaces without defects such as steps and facets, and was also applied to the large-grained, high-purity iron sheets.

The plating solution contained 1.0 M $ZnSO_4 \cdot 7H_2O$ and 0.5 M Na_2SO_4 as a supporting electrolyte in distilled water which was essentially free of organic contaminants. The pH of the plating solution, maintained at 60° C, was adjusted to 2.0 by addition of some sulphuric acid. The electrodeposition was carried out galvanostastically at 60° C, and the electrical charge transferred during the deposition, was monitored by means of a coulometer (Hokuto Denko, HF-201). The current density was controlled at an appropriate level between 10 mA cm^{-2} and 2 A cm^{-2} by means of a galvanostat (Hokuto Denko, HA-111).

Examination of the prepared substrate surfaces and the plated specimen was carried out by means of a scanning Auger electron multiprobe, (PHI-600), a scanning electron microscope, (JSM-840), and a transmission electron microscope (Hitachi-H700) operated at 200 kV. The specimens for TEM observation were prepared as follows. Firstly, thin foils of the substrate were made by a conventional twin jet polishing method. They were then conditioned by the second method and were coated with a thin layer of zinc (at 0.5 C cm^{-2}).

3. Results

3.1. *Surface condition of the substrate prior to the electrodeposition*

Fig. 1 shows the surface of substrates A and C. Substrate A exhibited considerable surface roughness introduced in the rolling process as well as by the etching effects in the HCl solution. Although substrate B was not examined because it was covered with a water film until electrodeposition, it was considered to be almost the same as substrate A. The surface of substrate C, however, was rather smooth and the number of

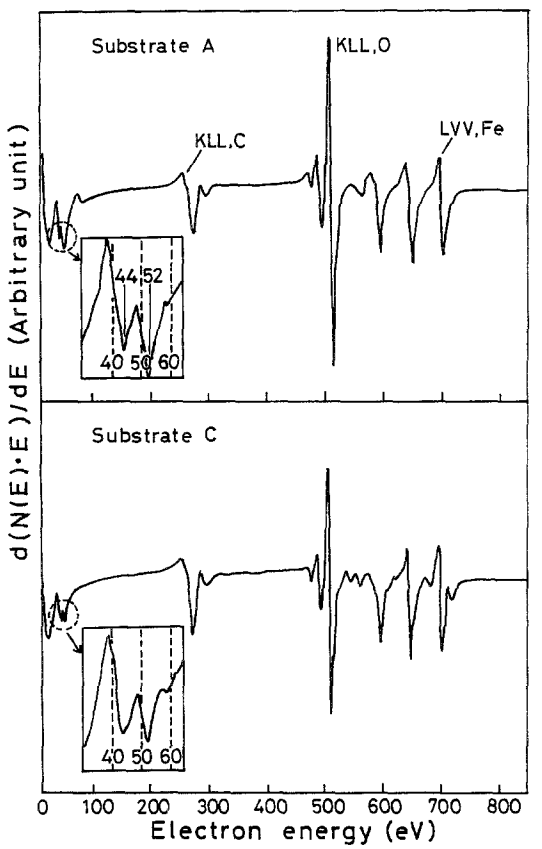

Fig. 2. Auger electron spectra of surfaces of substrates A and C.

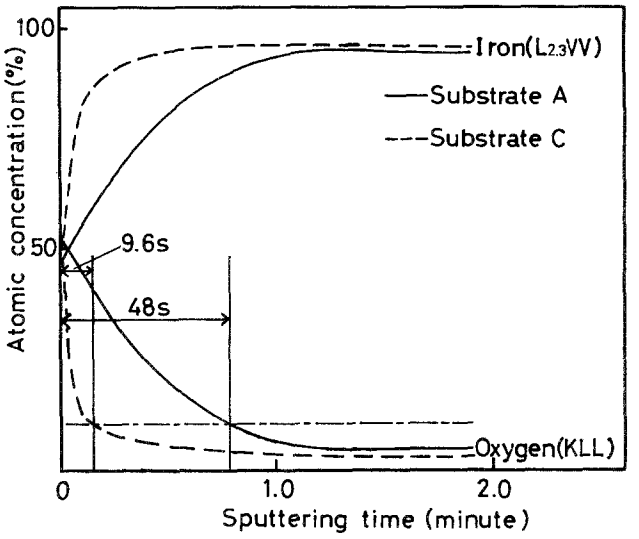

Fig. 3. Auger chemical depth profile of the oxidized surfaces of substrates A and C.

defects were fairly small. Fig. 2 shows Auger electron spectra obtained at the central area of Fig. 1a and b. In the case of substrate A, a strong oxygen KLL peak (581 eV), of which the height was about 250% of the iron LVV peak (701 eV), was observed. In addition, the carbon KLL peak observed was about 20% of the iron LVV peak. In the case of substrate C, the carbon KLL peak was higher and the oxygen KLL peak was much lower than those of substrate A.

The detailed Auger electron spectra in the low energy regions are also illustrated in Fig. 2. In both cases the iron LVV peaks (47 eV) were split into two peaks at 44 and 52 eV. This is due to the formation of iron oxide by oxygen adsorption from the air at room temperature [6–8]. Fig. 3a and b illustrates the chemical depth profile of the oxidized surfaces of substrates A and C. The ion current density used in the sputtering was kept at a constant value of 35 μA cm^{-2}. Atomic concentration was obtained by dividing the peak height by the relative sensitivity factor and was normalized by the total amount of oxygen and iron. In the case of substrate A the oxygen KLL peak decreased with increasing sputtering time, and reached the noise level after 48 s of sputtering. On the other hand the oxygen KLL peak of substrate C decreased fairly rapidly with sputtering time and reached the noise level after only 9.6 s of sputtering. These facts suggest that the thickness of the oxidized layer on substrate C is considerably thinner than that on substrate A.

3.2. *Morphology of zinc deposits*

Fig. 4 shows the morphologies of zinc crystals

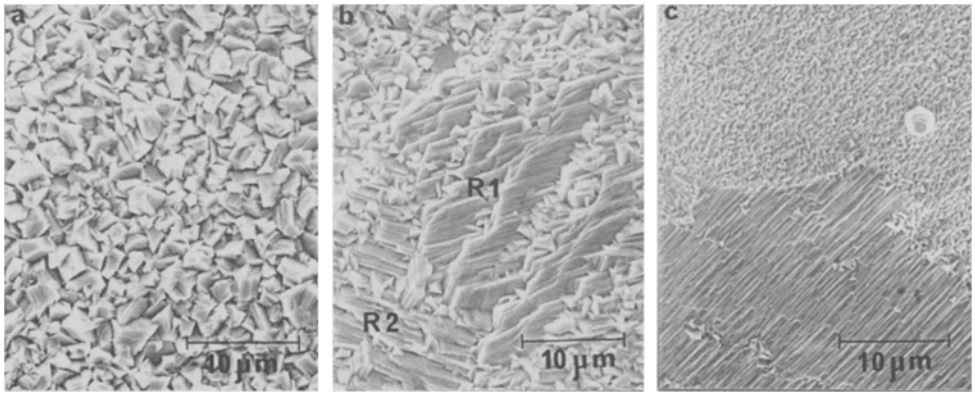

Fig. 4. Morphology of zinc crystals on substrates A (a), B (b) and C (c) at a current density of 500 mA cm^{-2}.

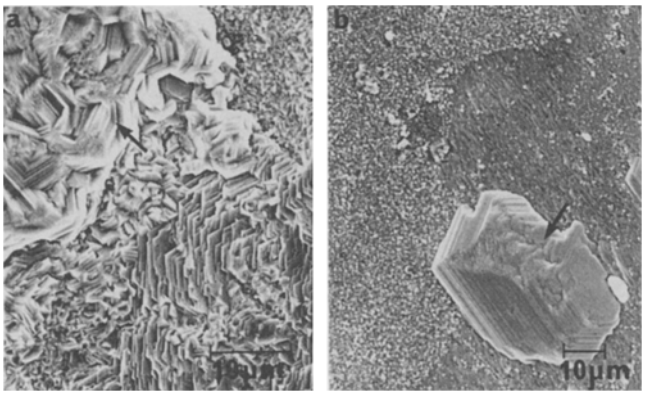

Fig. 5. Zinc crystals deposited at 10 mA cm^{-2} on substrates B (a) and C (b).

on substrates A, B and C at 10C cm^{-2}. Zinc crystals of substrate A were randomly oriented and showed homo-epitaxial growth on the basal plane (Fig. 4a). On substrate B, however, the morphology of the zinc deposits changed markedly from grain to grain of the ferrite substrate as indicated for the regions R1 and R2 (Fig. 4b). The interface separating R1 and R2 was confirmed to correspond to the grain boundary in the substrate. Zinc deposits on substrate B did not show a complete hetero-epitaxy and random growth regions were also observed. On substrate C the boundary separating the region of different morphology was clearly seen (Fig. 4c). It should be noted that the hetero-epitaxial growth of zinc crystals on substrate C was much closer to perfection than that on substrate B.

Figs 5 and 6 show the effects of current density on the hetero-epitaxial growth of the zinc deposits. At current densities from 10 to 500 mA cm^{-2}, hetero-epitaxial growth was observed on both substrates B and C. At the lowest current density of 10 mA cm^{-2}, where little hydrogen formation occurred, however, some parts of the epitaxial domain showed abnormal growth, and significant surface roughness occurred as shown in Fig. 5a and b (indicated by arrows). Even at the rather high current density of 1 A cm^{-2}, where aggressive hydrogen formation occurred, zinc deposits nucleated and grew hetero-epitaxially on both substrates B and C. At 2 A cm^{-2}, zinc deposits grew randomly and hetero-epitaxy disappeared on substrate B, although it still occurred on substrate C as shown by Fig. 6a and b.

Fig. 7 illustrates the zinc crystals deposited on the pure iron (1 0 0) surface polished chemically. Zinc crystals exhibited a cross-hatched morphology due to hetero-epitaxy (Fig. 7a), and the observation at a higher magnification (Fig. 7b) revealed four equivalent variants of the zinc–substrate orientation relationship. The crystallographic relationship between the deposits and the substrate was determined by comparing the morphology of the zinc crystals with the

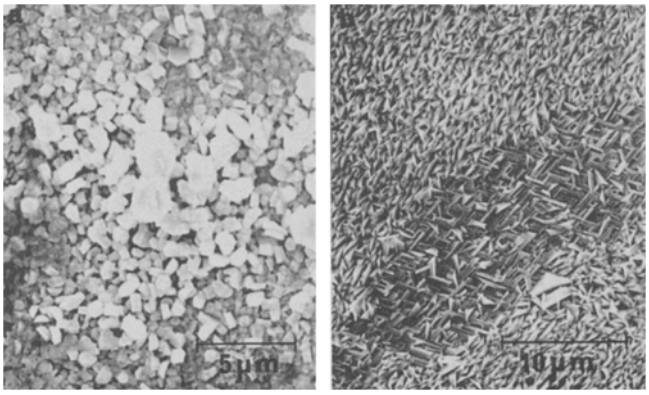

Fig. 6. Zinc crystals deposited at 2 A cm^{-2} on substrates B (a) and C (b).

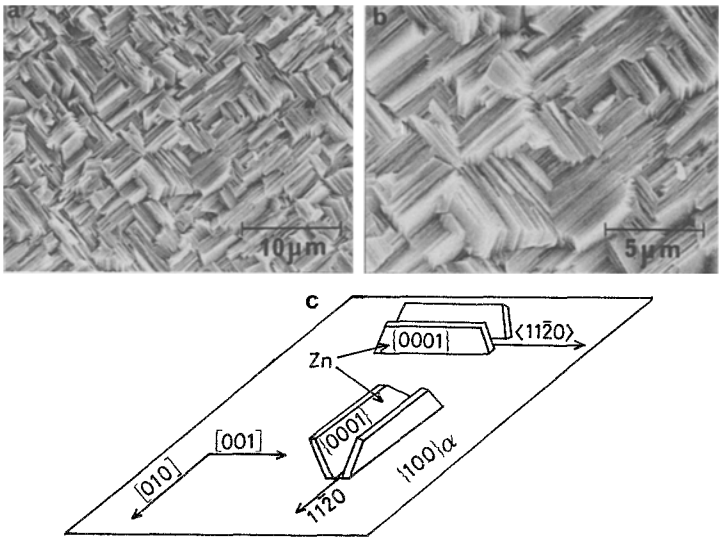

Fig. 7. Morphology of zinc deposits on (1 0 0) pure iron surface polished chemically. (a) SEM micrograph. (b) Higher magnification of (a). (c) Schematic illustration showing four variants of zinc–iron orientation relationship.

electron channelling pattern of the substrate, and is shown schematically in Fig. 7c.

3.3. *TEM observation of zinc deposits on substrates*

Zinc crystals deposited at 500 mA cm^{-2} on the thin film of a low-carbon steel sheet are shown in Figs 8 and 9. In the bright field image (Fig. 8), the dark regions due to the absorption contrast of zinc deposits were observed frequently, and exhibited sharp edges of thin hexagonal platelets (Fig. 9a). The selected area diffraction pattern from such a hexagonal edged region and its schematic representation provided the direct crystallographic orientation relationship between the zinc deposit and the ferrite. The dark field image (Fig. 9b), using a $(\bar{2}\,1\,1\,0)_{Zn}$ reflection beam, revealed that the hexagonal edged region did correspond to the zinc crystal. The crystallographic analysis of the electron diffraction pattern is shown in a stereographic projection in Fig. 10, where the following orientation relationship between both materials holds approximately.

$$(1\,1\,0)\alpha \parallel (0\,0\,0\,1)_{Zn}$$

$$(\bar{1}\,1\,1)\alpha \parallel (\bar{2}\,1\,1\,0)_{Zn}$$

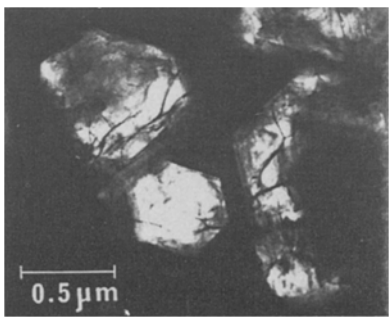

Fig. 8. Zinc deposits on the thin film of low-carbon steel.

4. Discussion

The surface condition of the substrates affects the hetero-epitaxy markedly as can be seen in Fig. 4, i.e. the c-axis of the zinc deposits showed random directions on substrate A, but the deposits grew hetero-epitaxially on substrates B and C. It seems reasonable to assume that the water film on substrate B largely reduced the oxidation on the substrate surfaces. In the case of substrate A, on the other hand, an iron oxide film, several hundred Angstrom thick, was formed, as shown by the Auger chemical depth profile. This suggests that the hetero-epitaxial growth is induced on the clean surface where zinc atoms can directly interact with substrate iron atoms and is disturbed by the oxide on the surface. It is interesting to note that almost perfect hetero-epitaxial growth was observed on substrate C, the surface of which was dried in air before deposition. This is probably explained by the fact that the thickness of the oxide on substrate C was very homogeneous and was about

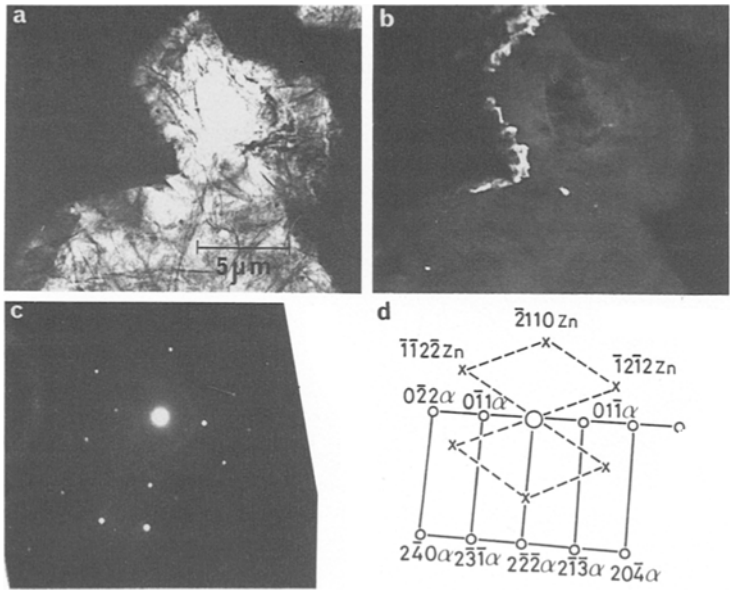

Fig. 9. Zinc deposits on the thin film of the steel. (a) Bright field image. (b) Dark field image using $(2\,1\,\bar{1}\,0)_{Zn}$ reflection. (c) Electron diffraction pattern of (a). (d) Schematic representation of (c).

a fifth of that on substrate A, i.e. the oxide film dissolves rapidly at the initial stage of deposition in low pH solution.

It should also be noted that hetero-epitaxial growth occurred on substrates B and C even at current densities as high as $1\,A\,cm^{-2}$, although previous work [6, 9–11] suggested dendritic or boulder-type growth at high cathodic overpotential. This indicates that the hetero-epitaxial growth mechanism is strongly affected by the surface chemical condition and the surface structure of the substrate.

Local disturbances in hetero-epitaxial growth were frequently observed on substrate B, whereas they did not occur on substrate C. This is probably due to the difference in the number of the

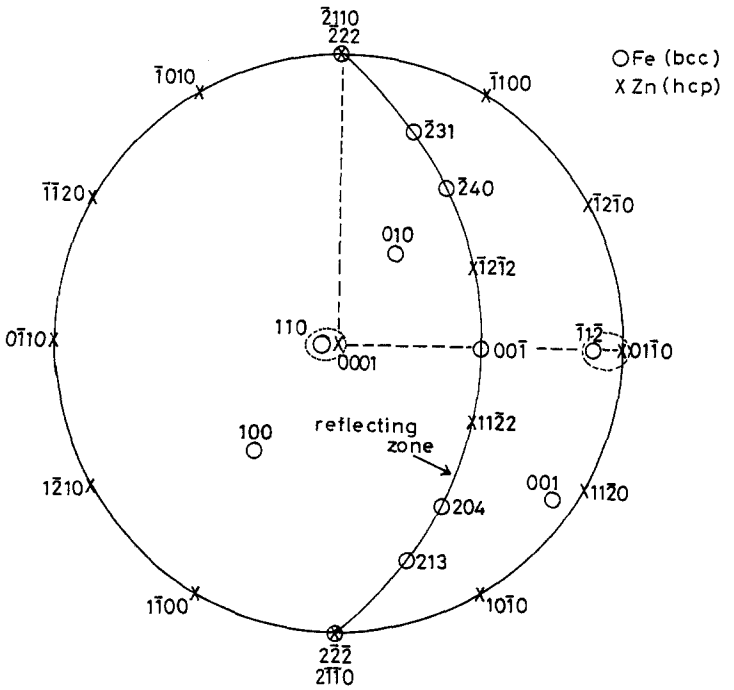

Fig. 10. Stereographic analysis of the diffraction pattern in Fig. 9.

defects such as facets and steps which were introduced during the rolling and pickling processes. In fact, the surface of substrate A was more severely corrugated than that of substrate C.

Thus, the present results show that the preparation of substrates is a very important factor for controlling the morphology of the deposits.

The orientation relationship between zinc crystals and the substrate iron in the present study is almost the same as that obtained by Takechi *et al.* [5], by texture analysis. Fig. 11 illustrates the lattice matching between zinc deposits and the substrate based on $(1\,1\,0)\alpha//(0\,0\,0\,1)_{Zn}$. A particularly good fit between both configurations along the $[\bar{1}\,1\,1]\alpha$ and $[\bar{2}\,1\,1\,0]_{Zn}$ is clearly seen.

5. Conclusions

The electrodeposition of zinc crystals on low-carbon steel sheets from sulphate solution has been studied in relation to the hetero-epitaxy between deposits and substrates.

1. The occurrence of hetero-epitaxial growth of zinc crystals on the substrate is largely affected by the surface condition of the substrate.

2. Increase in the thickness of the oxidized layers on the substrate surface prevents the hetero-epitaxial nucleation of zinc deposits.

3. In the case of thin oxidized layers, their dissolution in the early stage of electrodeposition may provide the direct interaction of zinc atoms with the substrate ferrite lattice and lead to hetero-epitaxial growth.

4. Surface roughness introduced during rolling and pickling processes also induces local disturbance in hetero-epitaxial growth.

5. The orientation relationship between zinc crystals and the ferrite is almost the same as that obtained by Takechi *et al.* [5], and this lattice matching induces hetero-epitaxy.

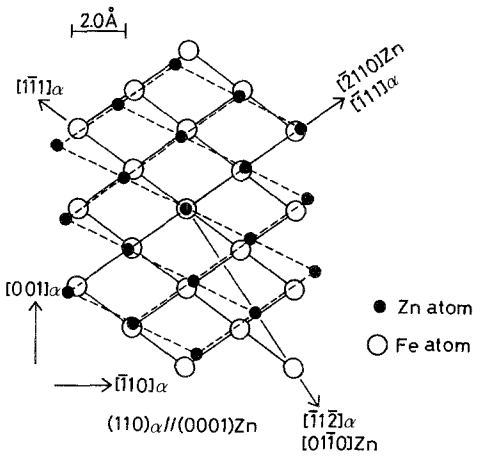

Fig. 11. Lattice matching between zinc deposits and the substrate.

Acknowledgements

The authors would like to thank Dr Y. Itoh, General Manager, and Dr T. Yukitoshi, Assistant General Manager of Technical Research Laboratories, Sumitomo Metal Industries, Ltd, for permission to publish this article. The authors are also grateful to Dr A. Shibuya for his valuable advice.

References

[1] J. O'M. Bockris, Z. Nagy and D. Drazić, *J. Electrochem. Soc.* **12** (1973) 30.
[2] S. Itoh, N. Yamazone and T. Seiyama, *Surf. Technol.* **5** (1977) 27.
[3] A. Tanaka, A. Nakayama, Y. Uyeda and F. Noguchi, *Jap. J. Metal* **44** (1980) 741.
[4] D. Lashmore, *J. Electrochem. Soc.* **127** (1980) 573.
[5] H. Takechi, M. Matsuo, K. Kawasaki and T. Tamura, 6th International Conference on Texture of Materials (Tokyo, September 1981), Iron and Steel Institute of Japan, p. 43.
[6] M. Suleman and E. B. Pattinson, *Surface Sci.* **35** (1973) 75.
[7] C. Leygraf and S. Ekelund, *ibid.* **40** (1973) 609.
[8] K. Ueda and R. Shimizu, *ibid.* **43** (1974) 77.
[9] D. T. Chin, R. Sethi and J. McBreen, *J. Electrochem. Soc.* **129** (1982) 2677.
[10] F. Mansfeld and S. Gilman, *ibid.* **117** (1970) 1521.
[11] R. D. Naybour, *ibid.* **116** (1969) 52.